INTERNATIONAL JOURNAL OF OPTIMIZATION IN CIVIL ENGINEERING
Int. J. Optim. Civil Eng., 2022; 12(4):557-575

A RESOLUTION-BASED APPROACH TO REFINE THE SEARCH SPACE FOR STRUCTURAL DAMAGE DETECTION

N. Sedaghati and M. Shahrouzi[*], [†]
Civil Engineering Department, Faculty of Engineering, Kharazmi University, Karaj, Iran

ABSTRACT

Beyond common practice that treats structural damage detection as an optimization problem, the present work offers another approach that updates boundaries of the damage ratios. In this approach the bandwidth between such lower and upper boundaries, is adaptively reduced aiming to coincide at the true damage state. Formulation of the proposed method is developed using modal strain energy in a system of finite elements. A resolution-based technique is applied so that the search space cardinality can be defined and then reduced. The proposed method is validated on different structural types including beam, frame and truss examples with various damage scenarios. The results exhibit high cardinality reduction and capability of the proposed iterative method in squeezing the design space for more efficient search.

Keywords: structural health monitoring; damage-boundary detection; search space reduction; modal strain energy; skeletal structures

Received: 10 July 2022, Accepted: 25 August 2022

1. INTRODUCTION

Structural Health Monitoring (SHM) is a rewarding task for practical engineering applications that have received considerable attention in recent decades [1,2]. In a major branch of SHM, damage detection techniques are utilized to evaluate the current state of an existing structure. A common approach in structural damage detection is formulating it as an inverse problem. It can be distinguished via the following levels [3]:
Level 1: Determining the damage occurrence in the structure

---

[*]Corresponding author: Civil Engineering Department, Faculty of Engineering, Kharazmi University, Tehran & Karaj, Iran
[†]E-mail address: shahruzi@khu.ac.ir (Mohsen Shahrouzi)

Level 2: Detecting geometry and location of the damage
Level 3: Quantifying severity of the damage
Level 4: Predicting the remained service life of the structure

Dynamic responses of a structure undergo changes due to variation of its mass, stiffness or damping properties. Structural damage causes loss of stiffness in one or more elements of the model and consequently affects its modal shapes and frequencies. However, it is difficult to localize the damage by mere use of the global dynamic properties. For example, spatial information about structural damage distribution may not generally be obtained by a single vibration frequency. Multiple frequency shifts, may better provide such spatial information, as variation of structural properties at different locations will cause different combinations of changes in the modal frequencies [4] .

Yuen examined variation of mode-shape and mode-shape-slope parameters [5]. Stubbs et al. [6] developed another damage detection method using sensitivity of modal frequency changes. The sensitivity equations for the entire dynamical system are rearranged as a system of algebraic equations with unknowns of stiffness losses at selected locations. Hearn and Testa [7] developed a damage detection method that examines the ratio of changes in natural frequency for various modes. Kam and Lee [8] presented an analytical formulation for locating a crack and quantifying its severity considering changes in the vibration frequency and mode shape. Richardson and Mannan [9] proposed a method that assumes that damage is limited to changes in the stiffness. The method requires pre-damage mode shapes, pre-damage frequency measurements, and post-damage frequency measurements. Balis Crema et al. [10] used the modal parameter sensitivity equations presented by Stubbs et al. [6] to locate damage They examined not only the effects of the location of the damage on successful damage detection but also the relationship between the modes used in the analysis and the position of the damage.

A number of investigators applied meta-heuristics to identify structural damage. Nobahari et al. [11] used a residual force function with genetic algorithm to identify damage in truss structures. Gomez and Silva [12] performed comparisons on application of genetic algorithms with modal data for this problem. Kang et al. [13], applied a hybrid particle swarm optimizer for damage detection of beam structures. A simplified dolphin echolocation algorithm was proposed by Kaveh et al. [14] using modal data of structures. Shahrouzi and Sabzi [15] introduced two hybrid variants of teaching-learning-based optimization and artificial immune system to identify damage in planar and spatial truss structures. Kaveh and Dadras [16] proposed structural damage identification by an enhanced thermal exchange optimization. Sarjamei et al. [17] studied structural damage detection using gold rush opimization algorithm. Ghannadi and Kourehli [18] applied a modified total modal assurance criteria in three recent meta-heuristics including multi-verse optimizer. Jiang et al. applied beetle swarm optimization algorithm for localizing and quantifying structural damage [19]. Kaveh et al. [20] developed a boundary-strategy to enhance damage identification in four different meta-heuristics including shuffled shepherd optimization algorithm.

The present work concerns modal strain energy relations [21–23] to derive a system of governing equations. It is furthermore used via a novel procedure to iteratively refine the upper and lower bounds on the damage ratios. A resolution-based strategy enables definition of search space cardinality so that its reduction can be further traced. The proposed method is applied on three examples of different types; including beam, frame and truss structures. In each case, single and multiple damage scenarios are treated to evaluate how the proposed method can squeeze the search space and by which resolution indices it can converge to the prescribed damage state.

2. GOVERNING EQUATIONS

For a structural system with the stiffness matrix of [K] and the mass matrix of [M], the eigenvalue problem is expressed as:

$$[K]\times\{\varphi_i\}=\omega_i^2[M]\times\{\varphi_i\} \tag{1}$$

In the typical i^{th} mode; the eigenvalue is square of the corresponding circular frequency ω_i and the mode shape vector is denoted by $\{\varphi_i\}$.

The damage state of a structural system is modelled by a stiffness loss in the corresponding element matrix as:

$$\left[K_e^d\right]=\left(1-\alpha_e\right)\left[K_e^u\right] \tag{2}$$

where α_e stands for the *Damage Ratio* (DR) of the e^{th} element that varies between 0 and 1. $\left[Ke^d\right]$ and $\left[Ke^u\right]$ denote the corresponding damaged and undamaged stiffness matrices, respectively. *Modal Strain Energy* (MSE) of an e^{th} element in the i^{th} mode is defined as:

$$MSE_{ie}=(\{\varphi_i\}^T\times\left[K_e\right]\times\{\varphi_i\})/(\{\varphi_i\}^T\times\left[M_e\right]\times\{\varphi_i\}),\qquad i=1\ to\,N_m\ ,\ e=1\ to\,N_e \tag{3}$$

The stiffness and mass matrices for the e^{th}-element in global coordinates are denoted by $\left[K_e\right]$ and $\left[M_e\right]$, respectively. The vector $\{\varphi_i\}$ stands for the i^{th} mode shape. Here-in-after, assume that the mode shapes that are normalized to the mass matrix; i.e.:

$$\{\varphi_i\}^T\times\left[M_e\right]\times\{\varphi_i\}=1 \tag{4}$$

Consequently, the modal strain energy of an e^{th} element in the i^{th} mode is simplified as:

$$MSE_{ie}=\{\varphi_i\}^T\times\left[K_e\right]\times\{\varphi_i\} \tag{5}$$

Summing the relation over elements, the total modal strain energy of the structure is obtained for the normalized i^{th} mode as:

$$MSE_i = \{\varphi_i\}^T \times \left[K\right] \times \{\varphi_i\} = \omega_i^2 \tag{6}$$

The modal strain energy for a healthy element *e* is calculated as:

$$MSE_{ie}{}^{u} = \left[\Phi_i{}^{u}\right]^T \times \left[K_e^{u}\right] \times \left[\Phi_i{}^{u}\right] \tag{7}$$

While for the damaged e^{th} element, it is given as follows employing true damaged i^{th} mode-shape:

$$MSE_{ie}{}^{dd} = \left[\Phi_i{}^{d}\right]^T \times \left[K_e{}^{d}\right] \times \left[\Phi_i{}^{d}\right] \tag{8}$$

In practical cases that stiffness of the damaged element is not known, MSE is approximated using the undamaged stiffness matrix as:

$$MSE_{ie}{}^{d} = \left[\Phi_i{}^{d}\right]^T \times \left[K_e{}^{u}\right] \times \left[\Phi_i{}^{d}\right] \tag{9}$$

Considering Eq.(2) we have:

$$MSE_{ie}^{dd} = (1-\alpha_e) \times MSE_{ie}^{d} \tag{10}$$

The total stiffness matrix is obtained by assemblying the corresponding element matrices; that gives:

$$\sum_e MSE_{ie}^{d} = MSE_i^{d} \tag{11}$$

Therefore, the damage ratios should satisfy the follwoing equation:

$$\sum_{e=1}^{N_e} \left((1-\alpha_e) MSE_{ie}{}^{d} \right) = (\omega_i{}^{d})^2 \tag{12}$$

Effective Modal Strain Energy, EMSE, for the e^{th} element at the i^{th} mode is defined as:

$$EMSE_{ie} = MSE_{ie}{}^{d} \,/\, (\omega_i^{d})^2 \tag{13}$$

Applying N_m modes of vibration, the aforementioned equations can be rearranged as:

$$EMSE_{ie} \times \alpha_e = \sum_{e=1}^{N_e} EMSE_{ie} - 1,\ i = 1, \ldots, N_m \tag{14}$$

3. THE PROPOSED METHOD OF DAMAGE-BOUNDARY DETECTION

Eq.(14) represents a system of linear equations with $\{\alpha_e\}$ as its unknowns. It cannot directly be solved for most practical cases when the number of equations does not coincide with the number of elements. But it can be used to update limits on $\{\alpha_e\}$ by the proposed *Damage-Boundary-Detection* (DBD) procedure. DBD algorithm is given via the following steps:

Step 1. Set the control parameters of the algorithm; including the small thresholds $\varepsilon, \delta, \gamma$.

Step 2. Initiate the structural model and the consequent mass matrix. Generate undamaged stiffness matrix of each element and assemble them in the total stiffness matrix of the structure.

Step 3. For N_m number of modes, solve eigenvalue problem to find the vibration properties. Set the iteration number *t* to 1. Denote the lower and upper bounds on the damage ratio of the element *e*, by $\alpha_e^{L,t}$ and $\alpha_e^{U,t}$, respectively.

Step 4. Determine $\{\varphi_i^{\,d}\}, \omega_i^{\,d}$ for the assigned damage scenario and normalize the mode shapes to the mass matrix.

Step 5. For the considered damage scenario, update Eq. (14) by computing *Effective Modal Strain Energy* for every e^{th} element at the i^{th} mode: $EMSE_{ie}$.

Step 6. For linear equation of Eq. (14) at every mode do:

- For each element *e* do:
  - Initiate $\alpha_h^{U,\text{t}}$ by $1-\varepsilon$ for $h \in \{1, 2, ..., N_e\} \wedge h \neq e$
  - Use Eq. (14) in the corresponding mode to update $\alpha_h^{L,\text{t}}$
- For each element *e* do:
  - By the updated $\alpha_h^{L,\text{t}}$ for $h \in \{1, 2, ..., N_e\} \wedge h \neq e$, solve Eq. (14) in the corresponding mode to update $\alpha_h^{U,\text{t}}$
  - Compute the bandwidth of the corresponding damage ratio as $\beta_e^t = \alpha_h^{U,\text{t}} - \alpha_h^{L,\text{t}}$

Step 7. Update α_h^L, α_h^U by the new values when fall within previous limits.

Step 8. If $\left|\alpha_e^{U,\text{t}} - \alpha_e^{L,\text{t}}\right| < \gamma$, take damage ratio of the corresponding element as:

$$\alpha_e = (\alpha_e^{L,t} + \alpha_e^{U,t})/2 \tag{15}$$

Step 9. Check the termination criteria:

- If $\forall e \in \{1, 2, ..., N_e\}$, $\left|\alpha_{ei}^{L,\text{t}} - \alpha_{ei}^{L,\text{t}-1}\right| < \gamma \;\wedge\; \left|\alpha_{ei}^{U,\text{t}} - \alpha_{ei}^{U,\text{t}-1}\right| < \gamma$,
  - then go to **Step 10**
  - otherwise
  - Increase the iteration number by 1

- go back to **Step 5**

Step 10. Announce the updated α_e^L, α_e^U and their mean as the final results.

Note that the upper limit is initiated as $\alpha_e^U = 1-\varepsilon$ to preserve $\alpha_e^U < 1$ and prevent instability in Eigen solution of Eq. (1). In cases that $EMSE_{ie}$ falls below a very small value; say $\gamma \times \max_e(EMSE_{ie}^t)$, it is suppressed (temporarily replaced by 0) during solution of Eq. (14) to avoid abnormal results.

For practical implementation of DBD, the range of $[\alpha_e^L, \alpha_e^U]$ is discretized to a finite sequence of $\{\alpha_e^L, \alpha_e^L+\varepsilon, \alpha_e^L+2\varepsilon, ..., \alpha_e^U\}$. The tiny interval ε is taken 10^{-r} where r is an integer *resolution index* for such a discretization. In another word, every DR is rounded to r floating points. Such a discretization, enables definition of the search space cardinality $\theta(t)$ for any iteration, t, as:

$$\theta(t) = \prod_{e=1}^{Ne} [1+(\alpha_e^{U,t} - \alpha_e^{L,t}) / \varepsilon] \tag{16}$$

It is evident that such a cardinality, exponentially grows with increasing the total number of elements N_e or the resolution index r.

The search space *Cardinality Reduction* (CR) is thus defined as the ratio of $\theta(t)$ over its initial value:

$$CR(t) = \theta(t) / \theta(1) \tag{17}$$

The smaller CR, the higher reduction of the search space is achieved. CR varies from 1 toward 0. The best CR is 0 when the lower and upper bounds on the damage ratio coincide with each other; i.e. $\alpha_e^L = \alpha_e^U = \alpha_e$. It is noteworthy to indicate that DBD requires just $2N_e.N_m$ evaluations at every iteration for a structure with N_e elements and N_m considered modes of vibration.

4. NUMERICAL SIMULATION

Examples in three structural types are considered to evaluate performance of the proposed DBD in cardinality reduction. They include a flexural beam, a two-story frame and a space truss. Different damage scenarios are concerned in each example; including damages in a single element or multiple-elements. Furthermore, to examine whether DBD can detect location and/or severity of the damages, an error index is defined between the true and the calculated damage states. It is given by:

$$Error = \sum_{e=1}^{N_e} \left| \alpha_e - \alpha_e^{true} \right| \tag{18}$$

For practical purposes, the control parameters of the algorithm are taken dependent to the resolution index; *r*, as $\varepsilon = 10^{-r}$, $\delta = 0.5\varepsilon$ and $\gamma = 0.1\varepsilon$. Each case is solved by altering the resolution index to study its effect on performance of the proposed DBD in refining the damage ratio boundaries and detecting the prescribed state of the damage.

4.1 12-element beam

For the first example, a flexural beam with 12 elements is considered as previously addressed in literature [24]. As evident in Fig. 1, the beam is fixed at both ends. It is constructed from steel with the density of $7870\,kg/m^3$ and the elasticity modulus of $207\,GPa$. Every element has identical length of $0.60\,m$, section area of $0.0016\,m^2$ and moment of inertia of $3.4133\times10^{-9}\,m^4$. Two damage scenarios are considered, as given in Table 1. The first scenario constitutes a single damaged element at the middle of the beam. Fig. 2 shows performance of the proposed method in this case using different resolution indices. It is observed that the location of damage is detected but the bounds on the damage ratio are affected by the applied resolution. Especially the lower bound of damage ratio is below its prescribed value for the resolution indices less than 4. Increasing the resolution index, both the lower and upper bounds approach true damage ratios. The matter is numerically confirmed by Table 2.

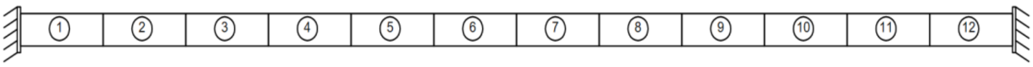

Figure 1. The 12-element clamped-clamped beam

Table 2: Damage ratios obtained by different resolutions for the 12-element beam

Damage Scenario	*e*	$r = 3$: α_e^L	$r = 3$: α_e^U	$r = 4$: α_e^L	$r = 4$: α_e^U
S1	6	0.1490	0.1500	0.1499	0.1500
	others	0.0000	0.0000	0.0000	0.0000
S2	6	0.0980	0.1000	0.0999	0.1000
	11	0.0990	0.1000	0.0999	0.1000
	others	0.0000	0.0000	0.0000	0.0000

e: Element Number, *r*: Resolution index

Table 3 reveals that the resolution index of $r = 4$ has resulted in CR of $10^{-10.8}$; that means more than 10 million times smaller search space with respect to $r = 3$. Table 4 confirms that the resulting error has decreased to the tiny value of 0.00005 for $r=4$, in this single-damage scenario. The least error for the multiple-damage in the 2nd scenario is obtained as 0.00010; that again corresponds to the highest applied resolution. Fig. 3 reveals that by $r=3$, DBD has just identified the location of damage; however, by applying $r=4$ its severity is also detected.

Table 1: Damage scenarios of the 12-element beam

Damage Scenario	e	α_e^{True}
S_1	6	0.15
S_2	6	0.10
	11	0.10

***e*:** Element Number

In the 2nd scenario,

Table 2: Damage ratios obtained by different resolutions for the 12-element beam

Damage Scenario	r = 3			r = 4	
	e	α_e^L	α_e^U	α_e^L	α_e^U
S1	6	0.1490	0.1500	0.1499	0.1500
	others	0.0000	0.0000	0.0000	0.0000
S2	6	0.0980	0.1000	0.0999	0.1000
	11	0.0990	0.1000	0.0999	0.1000
	others	0.0000	0.0000	0.0000	0.0000

e: Element Number, *r*: Resolution index

Table 3 declares that the applying $r=4$ has resulted in CR of $10^{-20.3}$; i.e. about 10^{10} times smaller search space than the other case in the same scenario. Furthermore, the multiple-damage scenario reveals better CR values than the single-damage scenario for every resolution index. It is confirmed by Fig. 4, where the curves of Log (CR) are plotted vs. iteration. It is observed that the higher the resolution, the more iterations are needed to converge.

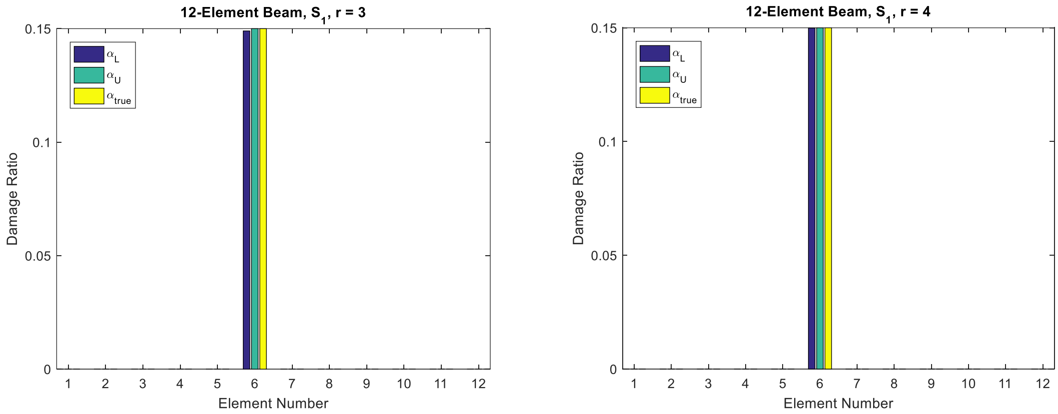

(a) (b)

Figure 2. The effect of increasing resolution in detection of damage scenario S_1 for the 12-element beam

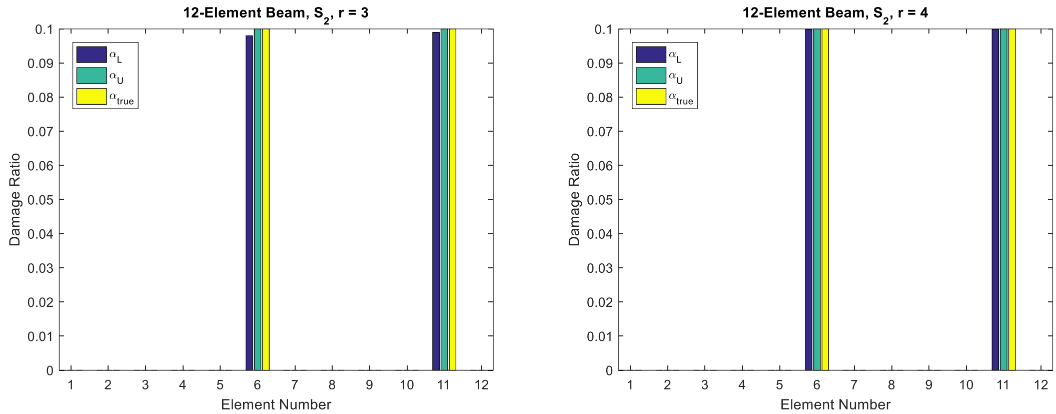

(a) (b)

Figure 3. The effect of increasing resolution in detection of damage scenario S_2 for the 12-element beam

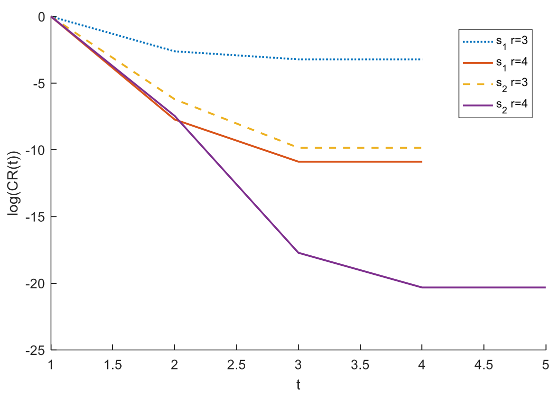

Figure 4. Cardinality reduction histories in damage detection of the 12-element beam

Table 2: Damage ratios obtained by different resolutions for the 12-element beam

Damage Scenario		$r = 3$		$r = 4$	
	e	α_e^L	α_e^U	α_e^L	α_e^U
S_1	6	0.1490	0.1500	0.1499	0.1500
	others	0.0000	0.0000	0.0000	0.0000
S_2	6	0.0980	0.1000	0.0999	0.1000
	11	0.0990	0.1000	0.0999	0.1000
	others	0.0000	0.0000	0.0000	0.0000

e: Element Number, *r*: Resolution index

Table 3: The resulted CR in damage detection of the 12-element beam

Damage Scenario	$r = 3$	$r = 4$
S_1	$10^{-3.2}$	$10^{-10.8}$
S_2	$10^{-9.8}$	$10^{-20.3}$

Table 4: The resulted *Error* in damage detection of the 12-element beam

Damage Scenario	$r = 3$	$r = 4$
S_1	0.00050	0.00005
S_2	0.00150	0.00010

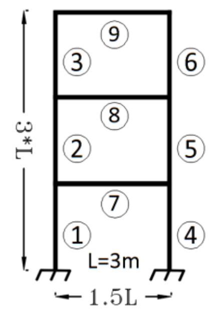

Figure 5. The 9-element planar frame

4.2 9-element moment frame

The multi-story steel moment frame of Figure 5 is treated with three degrees of freedom at each node. Modulus of elasticity, mass density, moment of inertia and cross sectional area for each element are $207\,GPa$, $7870\,kg/m^3$, $1.125\times10^{-7}\,m^4$ and $0.0015\,m^2$, respectively.

This example has already been studied with single and multiple-damage scenarios [24]. According to Table 5, in the first scenario the element 8 undergoes 15% stiffness loss while in the second 10% damage has occurred in the elements 4 and 8. An additional third scenario is also considered here, in which the elements 1, 4 and 7 experience stiffness losses of 10%, 15% and 20%, respectively.

Table 5: Damage scenarios of the 9-element frame

Damage Scenario	e	α_e^{True}
S_1	8	0.15
S_2	4	0.10
	8	0.10
S_3	1	0.10
	4	0.15
	7	0.20

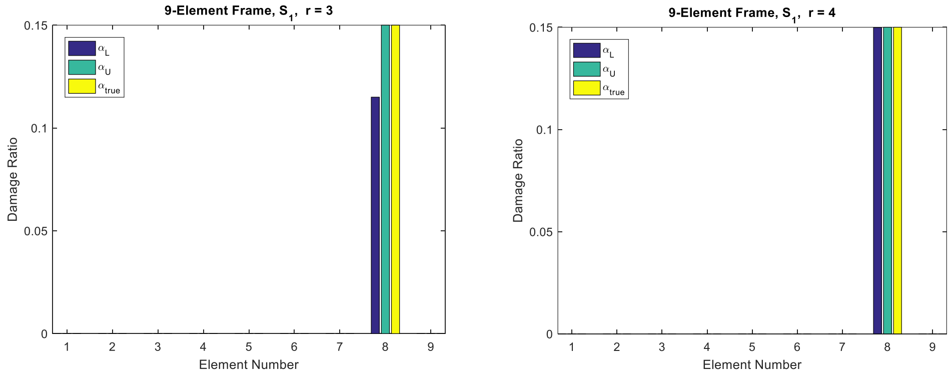

(a) (b)

Figure 6. The effect of increasing resolution in detection of scenario S_1 for the 9-element frame

In the first experiment, damage scenario S_1 is treated with the resolution of $r=3$. According to Fig. 6a, in this case the proposed DBD has successfully detected position of the damage (the element 8); however, the lower bound on the corresponding damage ratio α_8^L has not converged to true value of $\alpha_8^{true}=0.15$. Therefore, $r=3$ is not sufficient for detection of damage severity in this scenario. In the second experiment of scenario S_1, the resolution index is increased to 4.

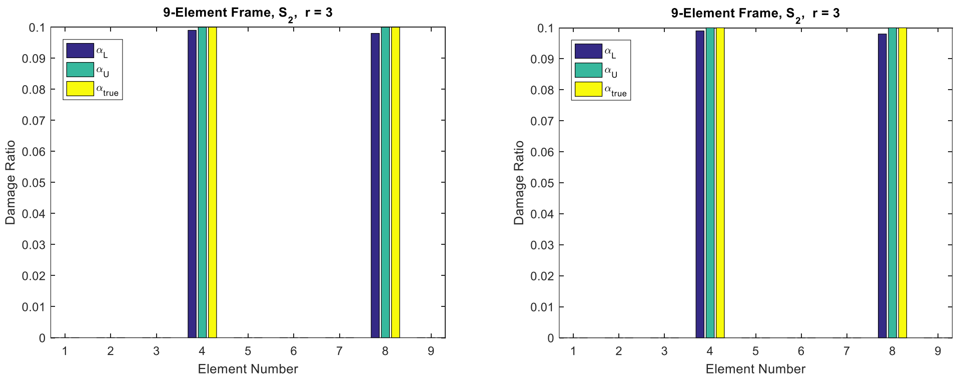

(a) (b)

Figure 7. The effect of increasing resolution in detection of scenario S_2 for the 9-element frame

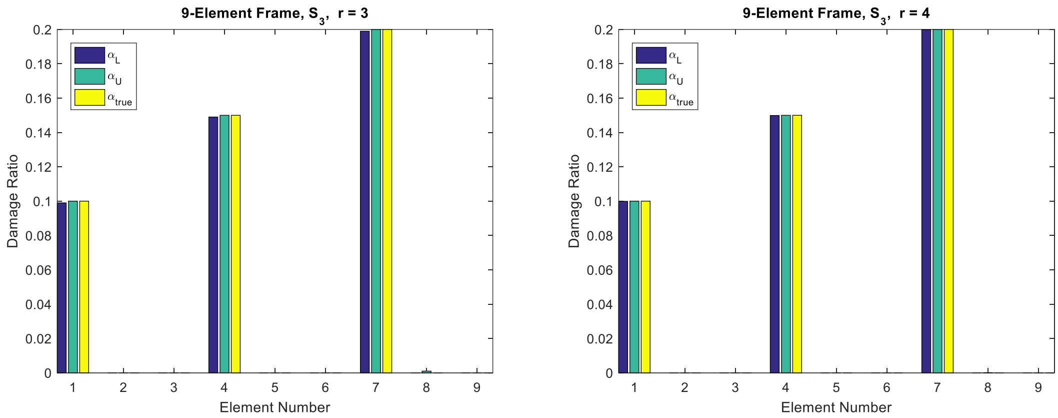

(a) (b)

Figure 8. The effect of increasing resolution in detection of damage scenario S_3 for the 9-element frame

According to Table 6 and Fig. 6b, in this case, the bounds on the damage ratio have converged to the value of 0.15 for the element 8 and 0.00 for the others. Finding location of true damage; i.e. the elements 1, 2 and 7 due to the 3rd scenario; is slightly violated by α_8^U of 0.001 in the case of the lower resolution $r = 3$. Comparison with the other case of $r = 4$, reveals that α_8^U is approaching zero by increasing such a resolution index. Note that in the 3rd scenario, the number of damaged elements over undamaged is as large as 50%. It is while DBD has successfully located the damage in the other two scenarios with lower ratio of damaged-to-undamaged elements.

Table 6: Damage ratios obtained by different resolutions for the 9-element frame

Damage		$r = 3$		$r = 4$	
Scenario	e	α_e^L	α_e^U	α_e^L	α_e^U
S_1	8	0.1150	0.1500	0.1499	0.1500
	others	0.0000	0.0000	0.0000	0.0000
S_2	4	0.0980	0.1000	0.0999	0.1000
	8	0.0990	0.1000	0.0999	0.1000
	others	0.0000	0.0000	0.0000	0.0000
S_3	1	0.0990	0.1000	0.0999	0.1000
	4	0.1490	0.1500	0.1499	0.1500
	7	0.1990	0.2000	0.1999	0.2000
	8	0.0000	0.0010	0.0000	0.0001
	others	0.0000	0.0000	0.0000	0.0000

Table 7: The resulted CR in damage detection of the 9-element frame

Damage Scenario	$r = 3$	$r = 4$
$\mathbf{S_1}$	$10^{-0.3}$	$10^{-3.2}$
$\mathbf{S_2}$	$10^{-8.3}$	$10^{-16.6}$
$\mathbf{S_3}$	$10^{-14.0}$	$10^{-22.9}$

Table 8: The resulted *Error* in damage detection of the 9-element frame

Damage Scenario	$r = 3$	$r = 4$
$\mathbf{S_1}$	0.01750	0.00005
$\mathbf{S_2}$	0.00150	0.00010
$\mathbf{S_3}$	0.00200	0.00020

Such experiments are repeated for the 2nd damage scenario. Fig. 7 reveals that by increasing the resolution index from 3 to 4, true damage state of this scenario is captured by DBD. Note that in the 2nd scenario two elements (with ID numbers 4 and 8) have undergone different damage ratios. Similar phenomena is observed for the 3rd scenario of this example in Fig. 8, where three elements experience linearly increased damage ratios.

Another issue to study is variation of the search space cardinality, in each case. According to Table 7, in the first damage scenario CR has decreased from $10^{-0.3}$ to $10^{-3.2}$ by increasing *r* from 3 to 4; that means nearly 800 times smaller search space. Such reduction is obtained $10^{8.3}$ times for the 2nd scenario and $10^{8.9}$ times for the 3rd. So the amount of search space reduction by DBD depends on the given damage scenario. Note that in this example, CR has been more reduced for multiple-damage scenarios with respect to the single-damage (the first) scenario.

Fig. 9 compares CR convergence curves for different resolution of the treated scenarios, in logarithmic scale. It can be realized that in the 1st damage scenario DBD has converged in 2 iterations for $r = 3$ and in 3 iterations for $r = 4$. Switching to the next scenario, the number of iterations to converge differs, as in Fig. 9. In this example, for a specific resolution index, better CR reduction is observed for the damage scenario S_3 with respect to S_2 and also for the damage scenario S_2 with respect to S_1. Note that the number of damaged elements, is 1, 2 and 3 for the damage scenarios S_1, S_2 and S_3, respectively.

More intense study on finding damage state of each scenario, is briefed in Table 8. In the 1st damage scenario, such an error is significantly decreased from 0.01750 to 0.00005 by increasing the resolution index from 3 to 4, respectively. Similar decrease of error by increasing resolution in DBD, is observed for the 2nd and 3rd damage scenarios of this example; however, the amount of errors vary case by case depending on the scenario.

For any fixed resolution, the scenarios with more damaged elements has resulted in larger error. For example in the 3rd scenario with $r = 4$, DBD has led to the error of 0.00020 that may be considered sufficiently small; however, the errors of the 2nd and the 1st scenarios are even smaller. Nevertheless, increasing the resolution index to $r = 5$, improves such an error to 0.00002 and CR to $10^{-31.9}$ within just 8 iterations to converge.

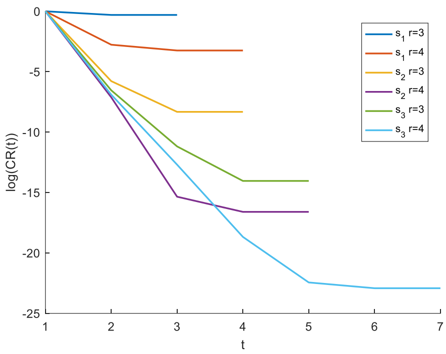

Figure 9. Cardinality reduction histories in damage detection of the 9-element frame

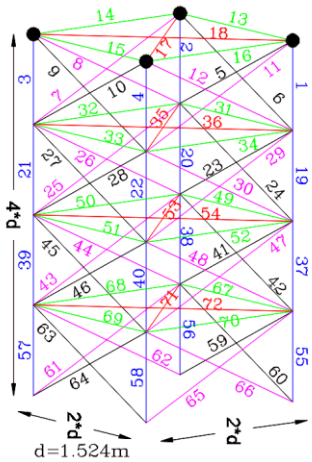

Figure 10. 72-bar spatial truss

4.3 72-bar spatial truss

As an example of spatial pin-jointed structures, the 72-bar truss of Fig. 10 is considered here. It has already been studied by a several investigators [14,25,26]. Material density is taken 2770 kg/m² while its elasticity modulus is 69.8GPa. Every member is constructed from a section with area of 0.0025 m². Non-structural mass of 2270 kg is attached to each of the four top nodes. Geometry and topology of the truss is demonstrated in Fig. 10. The corresponding damage scenarios are listed in Table 9.

Table 9: Damage scenarios of the 72-bar truss

Damage Scenario	e	α_e^{True}
S_1	55	0.15
S_2	4	0.10
	58	0.15
S_3	4	0.10
	14	0.13
	58	0.15

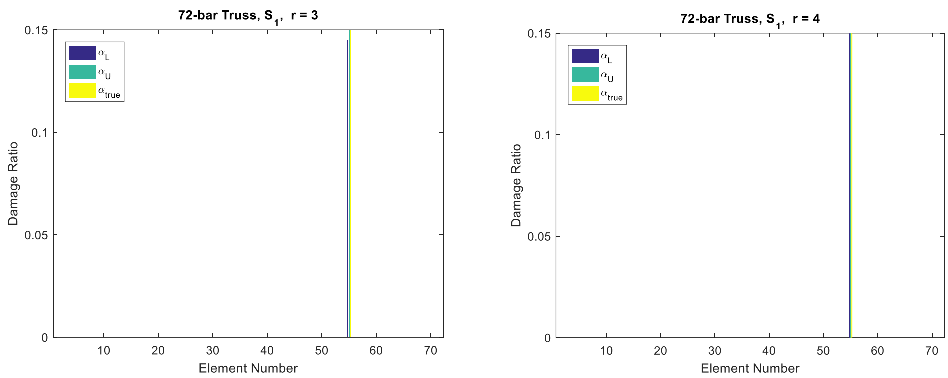

(a) (b)

Figure 11. The effect of increasing resolution in detection of damage scenario S_1 in the 72-bar truss

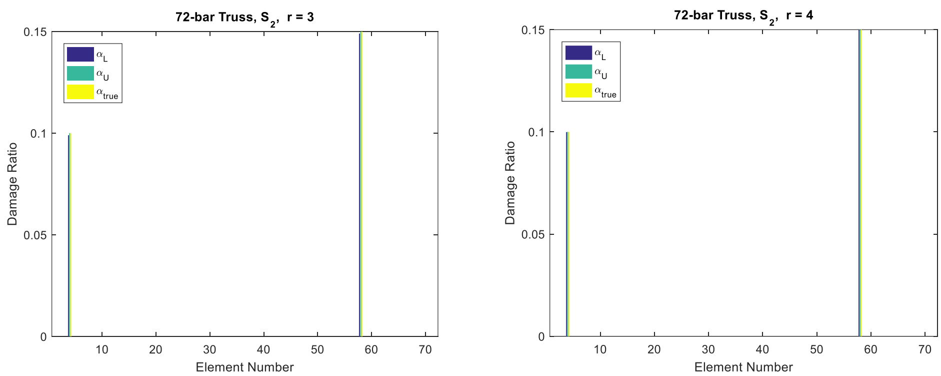

(a) (b)

Figure 12. The effect of increasing resolution in detection of damage scenario S_2 in the 72-bar truss

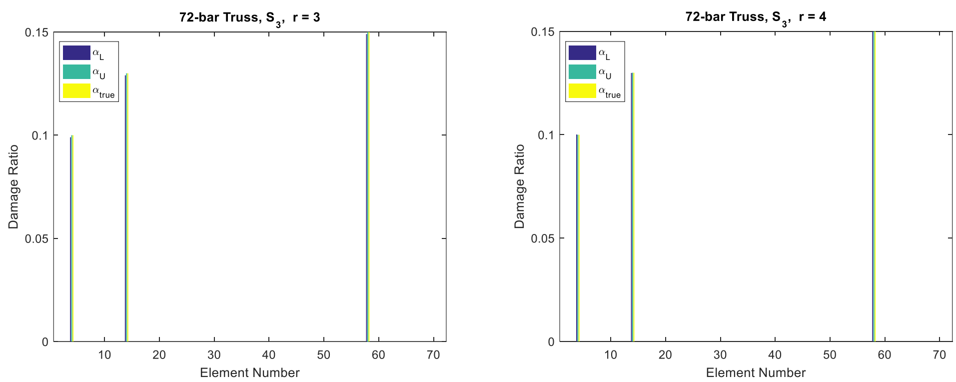

(a) (b)

Figure 13. The effect of increasing resolution in detection of damage scenario S_3 in the 72-bar truss

Table 10: Damage ratios obtained by different resolutions for the 72-bar truss

Damage Scenario	e	r = 3 α_e^L	r = 3 α_e^U	r = 4 α_e^L	r = 4 α_e^U
S_1	55	0.1450	0.1500	0.1499	0.1500
	others	0.0000	0.0000	0.0000	0.0000
S_2	4	0.0990	0.1000	0.0999	0.1000
	58	0.1490	0.1500	0.1499	0.1500
	others	0.0000	0.0000	0.0000	0.0000
S_3	4	0.0990	0.1000	0.0999	0.1000
	14	0.1290	0.1300	0.1299	0.1300
	58	0.1490	0.1500	0.1499	0.1500
	others	0.0000	0.0000	0.0000	0.0000

Table 11: The resulted CR in damage detection of the 72-bar truss

Damage Scenario	r = 3	r = 4
S_1	$10^{-6.0}$	$10^{-16.7}$
S_2	$10^{-16.6}$	$10^{-31.6}$
S_3	10^{-20}	$10^{-38.6}$

Table 12: The resulted *Error* in damage detection of the 72-bar truss

Damage Scenario	r = 3	r = 4
S_1	0.00250	0.00005
S_2	0.00100	0.00010
S_3	0.00150	0.00015

The obtained damage ratios by DBD are compared for two different resolutions in Table 10. Note that in all cases, α_e^U has been the first to approach α_e^{True}. It is not the case for the resulted values of α_e^{True}; however, they get better by increasing the resolution index. The matter is better declared for multiple-damage scenarios (the 2nd and the 3rd) than for the first. Nevertheless, both lower and upper bounds on the damage ratios are obtained zero for the undamaged elements. The proposed method has been successful in capturing true damage locations using either resolution cases, in this example; as the number of damaged elements constitutes a small portion (4.2%) of total elements.

According to Table 11, increasing resolution from 3 to 4 leads to $10^{10.7}$ times smaller search space in the 1st scenario with just one damaged element. In the 2nd scenario (with two damaged elements), CR values are in a lower range. In this case, CR has been reduced from $10^{-16.6}$ to $10^{-31.6}$ for the resolution indices of 3 and 4, respectively. That corresponds to 10^{15} times smaller search space for the higher resolution. Such a cardinality reduction is obtained more than 10^{18} times for the 3rd scenario with three damaged elements.

Fig. 11 shows that DBD has better approached to the prescribed damage state of the 1st

scenario by higher resolution of 4 with respect to 3. According to Table 12, this case corresponds to the tiny error of 0.00005 while applying $r = 3$ results in considerably greater error of 0.00250. Similar trend is observed (Fig. 12) for the 2nd damage scenario, so that increasing r (from 3 to 4) decreases the resulting error (from 0.00150 to 0.00010). It is evident from Fig. 13 that the proposed method has truly localized damages in the scenario S_3; however, severity of the damage is better identified by the higher resolution; i.e. $r = 4$. Although error reduction due to increasing resolution is again observed in the 3rd scenario; the error values differ from the other two. In another word, the amount of error depends not only on the resolution but also on the applied damage scenario.

It is observed in Fig. 14 that for every scenario of damage, convergence curve of the higher resolution has fallen below the other. The picture reveals that more iterations are generally required to converge in higher resolutions. In the other hand, they brings about more cardinality reduction (less CR values) than lower-resolution cases.

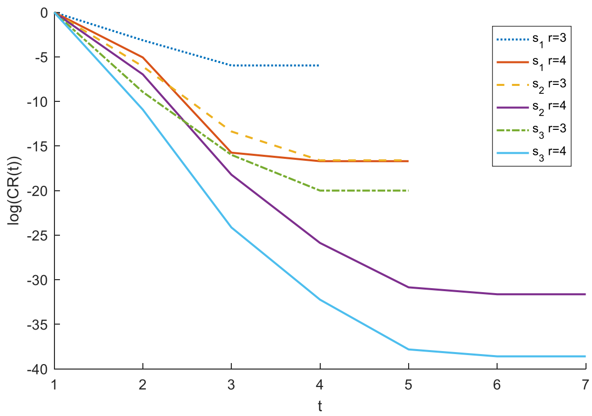

Figure 14. Cardinality reduction histories in damage detection of the 72-bar truss

5. CONCLUSION

Structural damage detection problem was reformulated using vibration data of the damaged state based on modal strain energy. As such a set of equations may include redundant number of unknowns, a novel method was offered to iteratively solve them by updating boundaries of the damage ratios. The proposed resolution-based technique made possible to measure the amount of search space reduction via CR, as well as accelerating convergence to the solution.

DBD was applied to a variety of structural types including beam, frame and truss examples. As a result, considerable search space reduction was observed starting from CR of $10^{-0.3}$ for the single-damage scenario in the 9-element frame example to $10^{-38.6}$ in a multiple-damage scenario of the 72-bar truss. Generally, the more the number of structural elements, the higher performance in search space reduction by DBD is observed.

The effect of resolution index was found quite considerable on such a cardinality reduction. Increasing the resolution index from 3 to 4 could result in 10^{7} to 10^{18} times smaller search space in various cases. In the other hand, higher resolution required more iterations to converge. Nevertheless, the number of such iterations was quite small; (less than 10) in the treated examples. It confirms capability of DBD in search space reduction by such a low computational effort.

In the light of our theoretical and numerical study, the proposed DBD was quite successful in achieving its main goal; that is to refine and squeeze the bandwidth between lower/upper bounds on the damage ratios. However, our experiments showed that the proposed DBD can identify the damage occurrence and location on various structures (beam, frame and truss) by taking into account all vibration modes. The results even exhibit ignorable errors in detecting severity of the damage when sufficiently high resolution is used in such cases. Further study on the effect of noisy or incomplete data is recommended as a future scope of research.

REFERENCES

1. Cho S, Jo H, Jang S, Park J, Jung HJ, Yun CB, Billie F. Spencer, Ju-Won Seo. Structural health monitoring of a cable-stayed bridge using wireless smart sensor technology: Data analyses, *Smart Struct Syst* 2010; **6**: 461–80. doi:10.12989/sss.2010.6.5_6.461.
2. Liu A, Wang L, Bornn L, Farrar C. Robust structural health monitoring under environmental and operational uncertainty with switching state-space autoregressive models, *Struct Heal Monit* 2019; **18**: 435–53. doi:10.1177/1475921718757721.
3. Farrar CR, Doebling SW. *An Overview of Modal Based Damge Identification Method*, Los Alamos National Laboratory, 1997.
4. Doebling SWS, Farrar CRC, Prime MBM, Shevitz DWD. *Damage Identification and Health Monitoring of Structural and Mechanical Systems from Changes in Their Vibration Characteristics: A Literature Review*, Los Alamos Natl Lab 1996: 133p. doi:10.2172/249299.
5. Yuen MMF. A numerical study of the eigenparameters of a damaged cantilever, *J Sound Vib* 1985; **103**: 301–10.
6. Stubbs N, Broome TH, Osegueda R. Nondestructive construction error detection in large space structures, *AIAA J* 1990; **28**: 146–52. doi:10.2514/3.10365.
7. Hearn G, Testa RB. Modal analysis for damage detection in structures, *J Struct Eng* (United States) 1991; **117**: 3042–63. doi:10.1061/(ASCE)0733-9445(1991)117:10(3042).
8. Kam TY, Lee TY. Detection of cracks in structures using modal test data, *Eng Fract Mech* 1992; **42**: 381–7. doi:10.1016/0013-7944(92)90227-6.
9. Richardson MH, Mannan MA. Correlating minute structural faults with changes in modal parameters, *11th International Modal Analysis Conference* 1993, pp. 893–898.
10. BalisCrema L, Castellani A, Coppotelli G. *Generalization Of Non-Destructive Damage Evaluation Using Modal Parameters*, SPIE Int Soc Opt Eng 1995: 428–34.
11. Nobahari M, Ghasemi MR, Shabakhty N. Truss structure damage identification using residual force vector and genetic algorithm, *Steel Compos Struct* 2017; **25**: 485–96. doi:10.12989/scs.2017.25.4.485.
12. Gomes HM, Silva NRS. Some comparisons for damage detection on structures using genetic algorithms and modal sensitivity method, *Appl Math Model* 2008; **32**: 2216–32.

doi:10.1016/j.apm.2007.07.002.
13. Kang F, Li J, Xu Q. Damage detection based on improved particle swarm optimization using vibration data, *Appl Soft Comput* 2012; **12**: 2329–35. doi:10.1016/j.asoc.2012.03.050.
14. Kaveh A, Rohollah S, Vaez H, Hosseini P, Fallah N. Detection of damage in truss structures using Simplified Dolphin Echolocation algorithm based on modal data, *Smart Struct Syst* 2016; **18**: 983–1004. doi:http://dx.doi.org/10.12989/sss.2016.18.5.983.
15. Shahrouzi M, Sabzi AH. Damage detection of truss structures by hybrid immune system and teaching–learning-based optimization, *Asian J Civil Eng* 2018; **19**: 811–25. doi:10.1007/s42107-018-0065-9.
16. Kaveh A, Dadras A. Structural damage identification using an enhanced thermal exchange optimization algorithm, *Eng Optim* 2018; **50**: 430–51. doi:10.1080/0305215X.2017.1318872.
17. Sarjamei S, Massoudi MS, EsfandiSarafraz M. Damage detection of truss structures via Gold Rush Opimization algorithm, *Int J Optim Civil Eng* 2022; **12**: 719–22. doi:10.1201/b18175-288.
18. Ghannadi P, Kourehli SS. Multiverse optimizer for structural damage detection : Numerical study and experimental validation, *Struct Des Tall Spec Build* 2020: 1–27. doi:10.1002/tal.1777.
19. Jiang Y, Wang S, Li Y. Localizing and quantifying structural damage by means of a beetle swarm optimization algorithm, *Adv Struct Eng* 2021; **24**: 370–84. doi:10.1177/1369433220956829.
20. Kaveh A, Hosseini SM, Zaerreza A. Boundary strategy for optimization-based structural damage detection problem using metaheuristic algorithms, *Period Polytech Civil Eng* 2020; **65**: 150–67. doi:10.3311/PPci.16924.
21. Srinivas V, Ramanjaneyulu K, Jeyasehar CA. Structural Health Monitoring 2011, doi:10.1177/1475921710373291.
22. Ghasemi MR, Nobahari M, Shabakhty N. Enhanced optimization-based structural damage detection method using modal strain energy and modal frequencies, *Eng Comput* 2018; **34**: 637–47. doi:10.1007/s00366-017-0563-5.
23. Shi ZY, Law SS, Zhang LM. Structural damage localization from modal strain energy change, *J Eng Mech* 2000; **126**: 1216–23. doi:10.1006/jsvi.1998.1878.
24. Moradipour P, Chan THT, Gallage C. An improved modal strain energy method for structural damage detection, 2D simulation, *Struct Eng Mech* 2015; **54**: 105–19. doi:10.12989/sem.2015.54.1.105.
25. Pholdee N, Bureerat S. Structural health monitoring through meta - heuristics - comparative performance study, *Adv Comput Des* 2016; **1**: 315–27. doi:http://dx.doi.org/10.12989/acd.2016.1.4.315.
26. Ghiasi R, Ghasemi MR. Optimization-based method for structural damage detection with consideration of uncertainties- a comparative study, *Smart Struct Syst* 2018; **22**: 561–74. doi:https://doi.org/10.12989/sss.2018.22.5.561.